Supporting Information

69451 Weinheim, Germany

DNA Reaction-Diffusion Attractor Patterns

Phillip J. Dorsey, Dominic Scalise, and Rebecca Schulman*

Abstract: Living systems can form and recover complex chemical patterns with precisely sized features in the ranges of tens or hundreds of microns. We show how designed reaction-diffusion processes can likewise produce precise patterns, termed attractor patterns, that reform their precise shape after being perturbed. We use oligonucleotide reaction networks, photolithography and microfluidic delivery to form precisely controlled attractor patterns and study the responses of these patterns to different localized perturbations. Linear and 'hill'-shaped patterns formed and stabilized into shapes and at time scales consistent with reaction-diffusion models. When patterns were perturbed in particular locations with UV light, they reliably reformed their steady state profiles. Recovery also occurred after repeated perturbations. By designing the far-from-equilibrium dynamics of a chemical system, this study shows how it is possible to design spatial patterns of molecules that are sustained and regenerated by continually evolving towards a specific steady state configuration.

DOI: 10.1002/anie.2016XXXXX

Table of Contents

Experimental Procedures

Reagents

All materials were purchased from commercial vendors and used as received. Poly(ethylene) glycol diacrylate (Avg. Mn = 575, 437441) was ordered from Millipore Sigma and camphorquinone (A14967) and triethanolamine (L04486) were ordered from Alfa Aesar. All oligonucleotides were purchased from Integrated DNA Technologies. All other reagents and materials are listed in the sections below detailing their use.

DNA strands used for in this paper are listed in Tables S1 and Table S2 along with the purification method. We annealed all complexes at the relative concentrations provided in Figure 2 of the main text. DNA complexes were annealed in Tris-acetate-EDTA buffer with 12.5 mM Mg^{2+}; the annealing protocol consisted of heating the solution up to 90 °C for 5 minutes and then cooling 1 °C every minute to 20 °C in an Eppendorf Mastercycler.

Table S1. DNA sequences used in linear pattern experiments listed from 5' to 3' direction. IDT chemical modifications are bracketed by / /.

Linear Pattern	Sequence	Purification
Linear Wire	CA TAACA CA TCT CA CAATC CA TCT CA CCACC CA	Desalted
Reporter Cover	CAATC CA TCT CA CCACC CA TCT CA/3BHQ_2/	HPLC
Reporter Bottom	/5Cy3/TG AGA TG GGTGG TG AGA TG GATTG TG AGA	HPLC
Reporter Bottom (used in some qPCR mixed experiments)	/56-FAM/TG AGA TG GGTGG TG AGA TG GATTG TG AGA	HPLC
Linear Competitor Cover	TA CA TCT /iSpPC/ CA CAATC CA TCT CA CCACC CA	HPLC
Linear Competitor Bottom	TG GGTGG TG AGA TG GATTG TG AGA TG TA	PAGE
Full Complement of Reporter	TCT CA CAATC CA TCT CA CCACC CA TCT CA	PAGE

Table S2. DNA strands for hill-shaped patterns listed from 5' to 3' direction. IDT chemical modifications are bracketed by / /.

Hill-shaped Pattern	Sequence	Purification
Hill Wire (Source Cover)	/5Cy3/CA TCT CA TAACA CA TCT CA CAATC CA TCT CA	HPLC
Source Bottom	TG ACATA TG AGA TG TGTTA TG AGA TG/3BHQ_2/	HPLC
Initiator	CA TCT CA TAACA CA TCT CA TATGT CA	PAGE
Sink Cover	T CA TAACA CA TCT CA CAATC CA TCT CA	PAGE
Sink Bottom	TG AGA TG GATTG TG AGA TG TGTTA TG AGA TG/3BHQ_2/	HPLC
Hill Competitor Cover	CA TCT CA/iSpPC/TAACA CA TCT CA CAATC CA TCT CA	HPLC
Hill Competitor Bottom (same as Sink Bottom)	TG AGA TG GATTG TG AGA TG TGTTA TG AGA TG/3BHQ_2/	HPLC
Sink/Competitor Bottom (noQ)	TG AGA TG GATTG TG AGA TG TGTTA TG AGA TG	Desalted

SUPPORTING INFORMATION

Microfluidic Device Design and Fabrication

The microfluidic network used in all experiments had the layout of the gradient generator previously described in Dorsey et al.[1] Each diffusion cell within the gradient generator was 1500 μm long, 50 μm in width, and 20 μm in height. Cells were grouped into arrays, each consisting of 5 cells with an inter-channel spacings of 50 μm; we designed each array of cells to fit exactly within the entire area of light projected (at 4X magnification) from a Polygon 400 DP digital micromirror array. Positive molds of SU-8 photoresist for the microfluidic device were fabricated on 4-inch silicon wafers using standard contact photolithography. Molds for the microfluidic device required two different heights of photoresist. Patterning this two-height device was achieved by first spin coating SU-8 10 (Microchem) to a target height of 20 μm, exposing the wafer to a UV dosage of 225 mJ/cm^2 (i-line), and then immersing it in SU-8 developer for 5-10 minutes. After confirming the integrity of the first stage of the mold, a second layer of SU-8 3050 (Microchem) was spin coated over the existing pattern for a target height of 100 μm. Care was taken to make sure that the alignment keys of the first patterned layer weren't covered by the second photoresist layer. These keys were used to align the wafer to the second photomask on a mask aligner. The same exposure dosage and development times described above were used to lift off un-crosslinked photoresist. The molds were then hard-baked overnight at 200 °C. Poly-dimethyl-siloxane microchannels were made by crosslinking Sylgard 184 (Dow-Corning) in a 10:1 ratio of base elastomer to curing agent. Wafers were used repeatedly to make PDMS devices; Sylgard 184 elastomer and crosslinker were mixed and then poured into a weigh boat holding the wafer. The mold was then degassed in a vacuum chamber to remove air bubbles. After thermally curing the PDMS mold for at least 2 hours at 70 °C, devices were removed from the mold, biopsy-punched to create device inlets and outlets, and cleaned in a UV-ozone oven with glass coverslips. Each device was bonded to a glass coverslip for 2 hours at 80 °C.

Digital Micromirror Array Operation

The digital light projection apparatus utilized in our experiments to photopolymerize hydrogels and perturb patterns consisted of a Mightex Systems Polygon 400 Dense Pixel array fitted into the light port of an inverted Olympus IX73 microscope. Blue light was routed from an LED through a liquid light guide and reflected off of the digital micro-mirror array into the light path of the microscope. We conducted all polymerizations with an Olympus 4X UPlan FL N 0.13 NA microscope objective, which resulted in a maximum exposed rectangular area of 1500 μm in width by 787 μm in height (height = 1.21 μm, width = 2.24 μm per pixel of projected light). We measured the intensity of 470 nm light at the sample stage to be 11.4 mW cm^{-2}; the intensity of UV light at 365 nm passed from a GreenSpot UV Curing system (GS2, America Ultraviolet Company) was 25 mW cm^{-2}. Each digital mask was designed in AutoCAD and rastered onto the digital micromirror array (DMD) through a software interface.

Reaction-Diffusion Hydrogel and UV Perturbation Setup

Before conducting polyethylene glycol diacrylate (PEGDA) photopolymerization within the microfluidic device, we treated the devices with a solution of 12% (v/v) 3-(trimethoxysily)propyl methacrylate (Millipore Sigma) in acidic methanol to functionalize the channel surface with pendant methacrylate groups in order to anchor the hydrogel to the surfaces of the channels. The pre-gel blend used in the experiments consisted of 30% (v/v) PEGDA 575 (Millipore Sigma), 0.5% (v/v) triethanolamine (TEA) (Alfa Aesar), 0.8% (w/v) (±) camphorquinone (CQ), and Tris-acetate-EDTA buffer with 12.5 mM magnesium acetate (TAE/Mg^{2+}). CQ was first dissolved in a 10% (w/w) solution of 1-butanol and diluted down to a final concentration of 0.8% (w/v) in order to promote its solubility in TAE/ Mg^{2+} buffer. The photopolymerization was conducted for 20 s (228 mJ cm^{-2}) on each array of microchannels. Tygon tubing was then inserted into the outlet and inlets. The inlets were connected to two upstream reservoirs containing the DNA reactants for the pattern forming reaction in TAE/ Mg^{2+} buffer. A fluidic controller[2] provided constant pressure-driven flow of DNA oligonucleotides through both sides of the diffusion cells; liquid was routed through a resistor upstream of the diffusion cells to mitigate convection due to pressure imbalances on either side of the diffusion channels. Equal pressures of 1.3 PSI were applied to each reservoir.

Images were obtained via time-lapse fluorescence microscopy using a 16-bit Infinity 3 CCD camera at 400-900 ms exposures. During UV exposures, light from the blue LED was used to position the digital UV mask (500 μm or 100 μm width by 787 μm height) over the array. Light was then routed from a GreenSpot2 UV lamp into the Polygon 400 DP through a liquid light guide and exposed onto the array for a defined period of time. Imaging resumed immediately after UV exposure. Dark frame correction was performed on individual images to remove artifacts from uneven signal intensity across the CCD array. We constructed montages of the microchannel arrays by digitally appending individual images with overlapping fields of view and smoothing of the montage to remove residual noise.

SUPPORTING INFORMATION

Results and Discussion

1. Design of the hill-shaped pattern reaction network

The Source and Consumption reactions were designed to produce and degrade Hill Wire (HW) according to 0th order and 1st order reaction kinetics respectively. These kinetics were achieved using bimolecular reactions, while maintaining constant concentrations of the reactants used to produce and consume HW. At each location in space the reactions were designed so that the total flux of HW at each time point (excluding diffusion) obeys the following reaction rules:

$$\text{Source rate} = k_a[\text{Source}][\text{Initiator}] \approx k_p \quad (1)$$

$$\text{Consumption rate} = k_b[\text{Sink}][\text{Hill Wire}] \approx k_d[\text{Hill Wire}] \quad (2)$$

$$\frac{\partial[\text{Hill Wire}]}{\partial t} = k_p - k_d[\text{Hill Wire}] = k_d\left(\frac{k_p}{k_d} - [\text{Hill Wire}]\right) \quad (3)$$

The reaction network (equations 1 and 2) is designed so that it regulates the concentration of Wire in a manner similar the behavior of a negative-feedback proportional controller (equation 3) that resists changes in HW concentration. Here, k_a and k_b are the second order rate constants for the designed reactions and k_p and k_d represent the effective rate constants of Wire production and degradation when [Source], [Initiator] and [Sink] remain approximately constant during the experiment. In the analogy to a proportional controller, k_d and k_p/k_d are the controller gain and set-point respectively. The rate of growth and magnitude of the steady state profile of the HW patterns were then determined by the values of the constant concentrations of reactants in the system and the reaction rate constants. Specifically, in a spatial context, HW is produced at a particular location in space at a 0th order rate. HW is then degraded in a 1st order reaction as it diffuses away from its point source. The resulting shape of the profile is a hill, where the concentration of Wire decreases with increasing distance from the source of generation.

2. Cy3 Fluorophore insensitivity to UV light exposure in 30% PEGDA hydrogels

Prior to conducting pattern perturbation experiments, we identified Cyanine 3 as a DNA dye modification that exhibited minimal photobleaching when exposed to UV light. We used this dye to track patterns with minimal interference from the UV light used to perturb them. To measure the extent of photobleaching of Cy3 after UV exposure in a hydrogel, we formed linear gradients of the Reporter Bottom strand, which has an attached Cy3 dye (sequence, Table S1) in the microfluidic diffusion cells with a boundary condition of 200 nM of at the right-hand side. After the patterns reached steady state, cells were subjected to either 30 seconds, 1 minute, 5 minutes and 10 minutes (equivalent to the maximum exposure time across all experiments) of UV light (intensity = 25 mW cm^{-2}) across the entire channel length. We then measured the change in profile intensity along the channel as (Intensity After UV exposure(t) – Intensity before UV exposure)/(Intensity at Right Boundary) at different times after exposure. At all exposure dosages, the patterns exhibited minimal deviation relative to the concentration boundary condition (Figure S1).

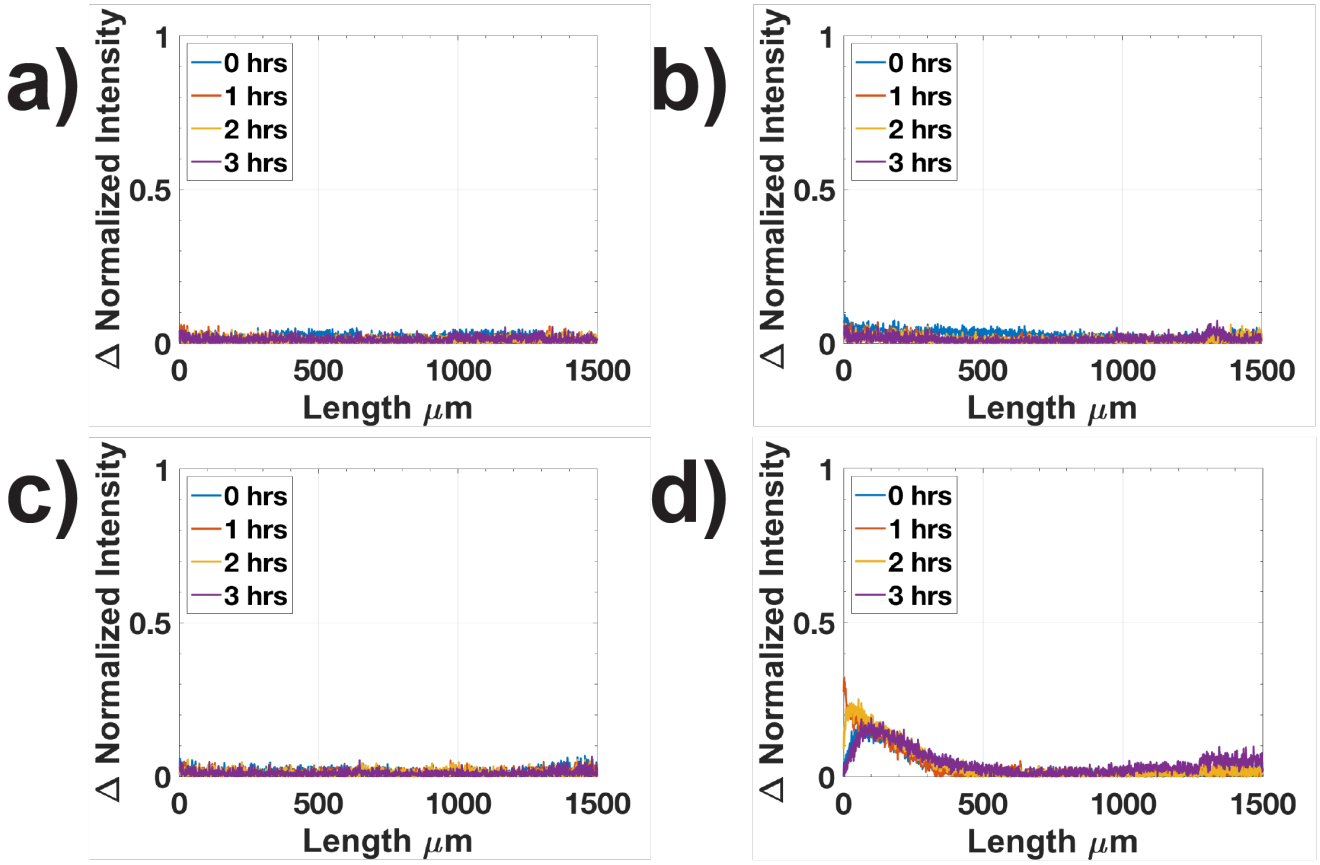

Figure S1. Changes in normalized profile intensity of a linear diffusive gradient of Reporter Bottom at different times after UV exposure a) 30 seconds, b) 1 minute and c) 5 minutes and d) 10 minutes. Δ normalized intensity = (Intensity After UV exposure (t) – Intensity before UV exposure)/(Intensity at Right Boundary).

3. The fluorescence intensity signal of the hill-shaped pattern contains artifacts due to Source fluorescence

During hill-shaped pattern formation, we observed that the fluorescence intensity at the boundary of a diffusion cell where Source entered was roughly 25% higher than the fluorescence intensity at than the opposite boundary; ideally the hill pattern should produce a concentration profile and resulting fluorescence intensity profile that is symmetric at both ends of the diffusion cell. The Source was functionalized with a fluorophore-quencher pair, whereas the species entering the diffusion cell from the opposite site had no fluorophores. We hypothesized that the difference in observed fluorescence intensities between the two boundaries was due to imperfect quenching of the fluorophore on the Wire strand while it was hybridized to Source Bottom (*i.e.* fluorescence from the Source complex). To test this hypothesis, we measured the fluorescence intensity of a gradient of Source complex by itself (Figure S2). We observed the formation a linear Source gradient with a difference in fluorescence intensity of roughly 2000 counts between its boundaries; this value was 25% of the typical peak hill intensities measured during an experiment which ranged from 8000-10000 counts in magnitude. This experiment demonstrated that the Source complex alone formed a linear gradient that was detectable within the diffusion cells and that the magnitude of this gradient was sufficient to explain the observed difference. We account for this artifact in our reaction-diffusion model of hill patterns (see Results & Discussion 5).

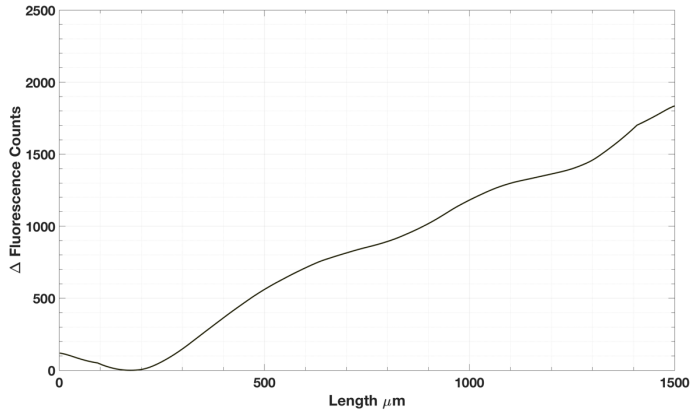

Figure S2. Raw fluorescence intensity profile of Source diffusing into a diffusion cell at 18 hours. 2.5 μM Source entered the hydrogel from the right-side boundary and was roughly 2000 counts higher than the left-side boundary. Here, the difference in Source gradient fluorescence intensity between left and right boundaries is shown. 2000 counts is roughly 25% of the typical peak hill intensity measured during an experiment which ranged from 8000-10000 counts in magnitude.

4. Characterization of leak reactions between species in Linear and Hill attractor patterns

Undesired side-reactions have the potential to influence the experimentally observed dynamics of formation of the linear and hill patterns. To understand how leaks resulting from undesired side reactions might impact the reaction-diffusion processes studied here, we first enumerated the side-reactions occurring between single stranded (ss) DNA and double stranded (ds) DNA species occurring through three-way branch migration. The potential reactions for each of the pattern systems are given in Figures S3 and S4 respectively. To understand the influence of these leaks, we measured the rates of key leak reactions, and the rates for some designed reactions, in well-mixed solution. All experiments discussed in the following section were conducted in 96-well plates in TAE/ Mg^{2+} buffer and in the presence of 10 μM of polyT20 DNA (to prevent surface adsorption between the DNA species and pipette tips or the plates) and were measured on a BioTek plate reader or Stratagene qPCR at 25 C.

Linear Patterns:

For linear patterns, we hypothesized that some of the Pre-Active Linear Competitor (PLC), containing the UV-cleavable linker, had been cleaved before the experiment and was therefore spuriously active. This spuriously active Linear Competitor (ALC) could sequester Linear Wire (LW) through its exposed toehold (we refer to spuriously generated ALC as either a complex containing a toehold cover that was cleaved and dissociated so that the bases of its toehold are exposed) (Figure S3, reaction 1). We sought to determine the rate constant of this leak reaction in well-mixed solution by measuring the degree to which the addition of different concentrations of PLC, which contained ALC and Inactive Linear Competitor (ILC), shifted the fluorescence intensity of a reversible LW-Reporter reaction that had been allowed to reach equilibrium. We mixed 20 nM of Reporter with 200 nM of LW in multiple wells of a 96-well plate. After the reaction reached steady state (as measured by a constant level of fluorescence intensity), we then added PLC to final concentrations of 0 to 1000 nM. This PLC solution presumably contained a proportion of ALC. After the addition of PLC, we observed a sharp drop in fluorescence intensity roughly proportional to the amount of PLC added (Figure S5), consistent with this hypothesis.

To measure the leak rate constant, kl4, of Reaction 1 in Figure S3, we had to determine the concentrations of Fluorophore and LW over time from measured fluorescence intensities. As such, we performed a calibration by mixing known amounts of Full Complement of the Reporter (FCR) with 20 nM Reporter, which is a standard practice for calibrating strand displacement reactions[3]. FCR reacts irreversibly with Reporter to release Fluorophore (R_f), and Quencher strands; we assumed that the concentration of Fluorophore was equal to the concentration of FCR added. To convert raw fluorescence counts into R_f, we first added 0 to 20 nM of FCR in separate wells, to 20 nM Reporter (Figure S6a). We then measured the change in fluorescence at steady state between: 5 nM and 0 nM FCR wells, 10 nM and 5 nM FCR wells, 15, nM and 10 nM FCR wells, 20 nM and 15 nM FCR wells, and 25 nM and 20 nM FCR wells. Each of these values was defined as α, which is the ratio of Δ [FCR]/Δcounts. We calculated the average value of α which provided a proportionality to convert raw counts to [R_f]:

$$\langle \alpha \rangle = \langle \frac{\Delta[FCR]}{\Delta Counts} \rangle \quad (4)$$

$$[R_f(t)] = \langle \alpha \rangle \Delta Counts(t) \quad (5)$$

To determine the concentration of LW from [R_f], we used the definition of the equilibrium constant and the known initial conditions of the reaction. We calculated the equilibrium constant after the reaction reached equilibrium using the initial concentrations of species and [$R_f(t_{eq})$]:

$$K_{eq}(t_{eq}) = \frac{[R_f(t_{eq})][Quencher_0 + R_f(t_{eq})]}{[Reporter_0 - R_f(t)][LW_0 - R_f(t_{eq})]} \quad (6)$$

After having determined K_{eq}, we calculated the average K_{eq} at steady state for the reversible reaction across the 5 well calibration conditions. We then used this calculated K_{eq} to calculate the concentration of LW(t) for all reaction wells:

$$LW(t) = \frac{[R_f(t)][Quencher_0 + R_f(t)]}{[Reporter_0 - R_f(t)]\langle K_{eq}\rangle} \quad (7)$$

Using this transformation, after 200 nM LW equilibrated with 20 nM Reporter, we then calculated the initial concentrations of Wire Quencher, Reporter from R_f at the time when PLC was added to the wells. We fit the kinetic traces following the time of PLC addition to a least-squares regression model (Figure S6a) where the fit parameters included the fraction of spuriously generated ALC and bimolecular rate constant for the LW/ALC leak reaction, kl4. The average fraction of ALC was estimated to be roughly 0.07 ± 3.0E-3 (95% confidence interval) of the total PLC concentration. The average value of kl4 was 1.47E6 ± 0.052 E6 M^{-1} s^{-1}(95% confidence interval), which is consistent with literature for the magnitude an effective 6-nt toehold rate constant[4]. As the toehold of PLC was 7 nucleotides in length, we assumed that our fitted parameter provided a reasonable estimate of the possible leak mechanism between ALC and LW.

Linear Competitor complex was annealed with 1.1X excess Linear Competitor Cover (LCC) to ensure that its reverse complement was entirely hybridized. We hypothesized that excess unbound LCC could possibly react reversibly with Reporter to generate a Fluorophore species and Quencher upon addition of the PLC to the reaction mixture. To determine whether this mechanism contributed to the measured experimental dynamics, we initially included Reaction 2 in our regression model. We observed that the fitted forward (kl5) and reverse (kl6) rate constants for Reaction 2 were on the order of 10^{-5} M^{-1} s^{-1} and 3E6 M^{-1} s^{-1}, which indicated that the optimal solution predicted by the model was a strongly reverse biased reaction. Additionally, the fitted rate constants were inconsistent with the 5-nt toehold size involved in the proposed mechanism, which should have been roughly ~ 10^4 M^{-1} s^{-1}, and none the fitted kinetic traces overlapped with the measured data. Based on these observations we surmised that the reaction mechanism was not strongly favored to occur and did not explain the dynamics we observed. It is possible that the presence of the 2-nitrobenzyl linker in the toehold of LCC contributed some degree of steric hindrance for the invading strand and limited the extent to which reaction 2 occurred. Therefore, the reversible 5-nt toehold reaction between Linear Competitor Cover (LCC) and Reporter (reaction 2 in Figure S3) was not included in our final model.

We also fit forward and reverse rate constants, kl1 and kl2, for the Reporting reaction using the reverse calibration kinetic traces (Figure S6b). The average values of kl1 and kl2 were 6.4E4 ± 0.5E4 M^{-1} s^{-1} and 2.6E5 ± 0.3E5 M^{-1} s^{-1}, which were within an order of magnitude of literature values for 5-bp length toeholds[4].It is important to note that the Reporter duplex possessed a quencher and fluorophore at its duplex end. This pair terminated the end of toehold binding domain for the reverse reaction (kl2); fluorescent dyes and quencher pairings are known to significantly stabilize the ends of DNA and RNA duplexes, effectively acting as an extra base-pair on the duplex[5,6]. Therefore, the magnitude of kl2 is reasonable because its toehold was effectively 6 nucleotides long.

Hill-shaped patterns:

For hill-shaped patterns, we enumerated key potential side reactions mainly occurring through three-way branch migration with Source, Competitor and Sink duplexes (Figure S4). Reaction 1 in Figure S4 could occur because Source complex was annealed with 1.1X excess Source bottom strand which could fully hybridize with Initiator, its reverse complement. The bimolecular rate constant for two single stranded oligonucleotides hybridizing to form a duplex in standard buffer conditions at 25 ºC has been characterized previously[4] to be 3.5E6 M^{-1} s^{-1}. We assumed kh8, the rate constant for this reaction, had this value.

Pre-active Hill Competitor (PHC) and Sink were annealed with 1.1X excess cover strands and these excess cover strands had the potential to react with the Source complex. Specifically, Inactive Hill Competitor (IHC) Cover could initiate a 0-nt toehold reaction with Source to form $Waste_2$ and produce Hill Wire (HW); this reaction can also proceed in the reverse direction through a 0-nt toehold initiated step. For reaction 3, Sink Cover could initiate a 0-nt toehold reaction with Source to generate Wire and $Waste_3$; this reaction was also reversible via a 0-nt toehold initiation step. To determine the importance of leak reactions 2 and 3, we measured the rates of the leak reactions involving IHC Cover, Sink Cover, and Source complex. We incubated varying concentrations of Sink complex and PHC complex with the same concentration of Source. The Sink or PHC complexes were annealed with 1.1X of the cover strand. In the strand displacement reactions used in the reaction-diffusion experiments, Sink and PHC and 3' quenchers terminated the ends of the duplexes. Upon hybridization of HW to these complexes, HW was not able to fluoresce because its 5' fluorophore was quenched by the 3' quencher on the Sink and PHC bottom strand. Importantly, to determine whether Sink and PHC complex reacted with Source in well-mixed conditions to generate HW, these complexes could not have 3' quenchers at their ends so that the leak reactions could be tracked using the fluorescence of HW once it had been displaced from Source Bottom. The Sink and PHC complexes used in these experiments lacked 3' quenchers so that the generation of free HW could therefore be measured in solution and would not be quenched by hybridization of Wire to IC or Sink complex (see Table S1 for sequence information).

To estimate the rate constant of Reaction 2, the fluorescence change over time was monitored after PHC was added to final concentrations ranging from 0 to 1 μM to solution containing 2.5 μM of Source (Figure S7a). To estimate the rate constant of Reaction 3, the fluorescence change was monitored over time after Sink was added to final concentrations ranging from 0 to 1.4 μM to solutions containing 2.5 μM of Source (Figure S7b). We then compared the fluorescence change in these reactions to the fluorescence change observed during an irreversible reaction of 0 to 2.5 μM of Initiator added to 2.5 μM of Source (Figure S7c). The increases in fluorescence 10 hours after each of the concentrations of PHC was added to Source were on order 50 counts, which was 0.1% of the steady state intensity generated by mixing 2.5 μM Initiator and Source (40,000 counts). Therefore, the amount of Wire generated by this reaction accounted for only 0.1% of the amount of HW generated by the reaction of 2.5 μM Source and

Initiator. The reaction of Sink and Source generated less than 200 counts across all concentrations of Sink added after 10 hours of measurement. This count change was less than 1% of the change in fluorescence intensity generated by the reaction of 2.5 μM Initiator and 2.5 μM of Source. The maximum concentrations of PHC and Sink used in these experiments were as large as the maximum concentrations used in the reaction-diffusion experiment; the measured rates of Reactions 2-3 should represent a maximum of the rates of these reactions in the hill pattern reaction-diffusion process. Therefore, the rates of Reactions 2-3 are small enough to be neglected in reaction-diffusion models of hill-pattern formation (see Results and Discussion 5).

In Reaction 4, excess IHC Cover reacted with Sink complex in a 4-nt toehold strand displacement reaction to generate IHC complex and Sink Cover. At the concentration of IHC complex mixed in the upstream reservoirs during pattern formation experiments (1 μM) there should be a maximum 100 nM of IHC Cover (if no spuriously cleaved AHC Cover is present) available to react with 1.4 μM Sink, resulting in a final reservoir Sink concentration of 1.3 μM upon completion of the reaction. This reaction was assumed to proceed with a 4-nt toehold rate constant of 5E3 M^{-1} s^{-1}, a standard value strand displacement reactions at 25 C in normal buffer conditions[4]. At this rate, the reaction of 1.4 μM Sink and 100 nM IC Cover would reach steady state roughly 12 minutes after initial mixing during reservoir preparation. As this time period was much shorter than the 1.5 hours of additional set up time following reservoir preparation, we neglected modeling this reaction in reaction-diffusion models and instead correct the boundary concentrations of Sink and IHC cover to their expected steady state values.

We also considered reactions in which non-UV exposed IHC could sequester HW. In this reaction, HW may bind to IHC and undergo strand displacement by hybridizing to exposed bases on IHC Bottom, which may become exposed because of reversible fraying of bases at the end of the duplex or 5' truncation errors in the toehold cover (Figure S4, reaction 5). Additionally, the 10 atom-length 2-nitrobenzyl linker whose length is the same as the length of approximately 3 bases, connected the 7-nt long toehold cover domain to the rest of Competitor Cover. Its presence in the phosphodiester backbone potentially disrupted local base stacking interactions and increased the rate of end fraying of the duplex. Spurious cleavage of the 2-nitrobenzyl linker resulting in the unbinding of the toehold cover could have also created an AHC species that could react with and sequester HW. Sequestration of HW could also occur because of some combination of these factors.

To classify the ways that the Pre-active Hill Competitor mixture might react with HW, we assumed that PHC was initially composed of two populations, Inactive (IC) Competitor and spuriously generated AHC. AHC refers to Hill Competitor that had its 2-nitrobenzyl linker photocleaved, and its cover dissociated, so that it could react rapidly with HW and sequester it via a 7-nt toehold-initiated reaction. IHC refers to Competitor that had its 2-nitrobenzyl linker intact and may or may not have had 5' truncation errors on its cover strand, possibly exposing a few end bases of the toehold to initiate binding of HW. AHC and IHC should sequester Wire at different rates; the AHC reaction proceeding with a rate constant for 7-nt toehold strand displacement reaction, on order 10^6 M^{-1} s^{-1} and IHC with an effective rate constant that reflects the collection of duplexes in truncated or frayed states with exposed toeholds, which we hypothesized would be on order of the rate constant for a toehold mediated strand displacement reaction initiated by a toehold of 0 ~ 4 nucleotides. The rate constant for the reaction between IHC and HW should therefore be several orders of magnitude lower than the rate constant for the reaction between AHC and HW. To measure these rate constants, we first compared the rates of reaction of HW with a PHC solution (which presumably also contained some AHC) and with a solution of AHC that was generated by exposing PHC to 302 nm UV light on a UVP bench top transilluminator for 30 minutes. We mixed 200 nM Source and 200 nM Initiator in multiple wells of a 96-well plate. After this reaction reached steady state, we added 0 to 1000 nM AHC or PHC separately to the wells and tracked the decreases in fluorescence over time (Figure S8). We observed rapid drops in fluorescence after the addition of AHC and the signal generated was completely quenched at AHC concentrations of 200 nM and higher (Figure S8a). For PHC, we observed an initial sharp decrease in fluorescence intensity followed by a slower decrease that appeared exponential in character (Figure S8b). The magnitude of the initial rapid fluorescence intensity decrease appeared roughly proportional to the concentration of PHC added, suggesting that PHC contained two populations of complex, one reacting quickly and the other reacting more slowly. These results supported the hypothesis that the PHC solution was composed of some fast-reacting AHC and IHC that reacted with HW at a slower rate.

We conducted experiments with lower concentrations of PHC, Source and Initiator to measure the effective reaction rate between IHC and HW and the fraction of AHC in a solution of PHC. We calibrated these reactions by measuring the change in fluorescence at steady state in the wells. First, 0 to 22 nM of Initiator was added to individual wells of 20 nM of Source. Similar to the FCR calibration we employed in the linear pattern system (SI Section 4 above), we then measured the fluorescence change at steady state between: 7 nM and 0 nM Initiator wells, 12 nM and 7 nM Initiator wells, 17 nM and 12 nM Initiator wells, and 22 nM and 17 nM Initiator wells. The average fluorescence change corresponded to a HW concentration change of 5 nM and allowed us to convert all fluorescence traces into a change in HW concentration.

The steps for measuring the leak rate constants proceed as follows. We mixed 20 nM Source and 22 nM Initiator in separate wells of a 96-well plate. After the irreversible reaction between Source and Initiator had gone to completion, PHC was added to each well to final concentrations of 5 to 100 nM (Figure S9). As we observed previously in experiments with higher concentrations of Source, Initiator and PHC, upon addition of PHC, the HW concentration in the wells initially dropped sharply then decayed more gradually over 17 hours of measurement. For each kinetic trace, we determined the fraction of AHC present within the Competitor mixture by calculating the ratio of the initial sharp decrease in HW concentration, HW_d, to the initial total concentration of PHC, $[HW_d]/[PHC]$. We assumed that the concentration of HW_d consumed corresponded to the concentration of AHC in the added PHC mixture; $[HW_d]/[PHC] = [AHC]/[PHC]$. The average fraction of AHC was 0.015 ± 0.09 (mean ± standard deviation). Having determined the initial fractions of IHC and AHC, we estimated the rate constants for slow (kh4) and fast (kh5) HW degradation reactions by fitting simulated kinetic traces to the experimental data using least-squares regression; the values of kh4 and kh5 were 1.1E3 ± 0.2E3 M^{-1} s^{-}

[1] and 2.5E5 ± 0.4E5 M^{-1} s^{-1} (95% CI) respectively. These rate constants were used in subsequent reaction-diffusion models of hill patterns and to model reactions 5 and 7 in Figure S4.

Importantly, we did not model the effects of toehold occlusion by photocleaved Competitor Cover on the toehold of AHC (Figure S4, reaction 6). Assuming the cleaved cover had a bimolecular rate constant of hybridization to the toehold of 3E6 M^{-1} s^{-1} (an established value for bimolecular rate constants of 7-nucleotide length) and that the toehold composition consisted equally of A/T and G/C nucleotide content, resulting in a free energy change of ΔG° = -9.2 kcal mol^{-1} upon hybridization, we calculated the fraction of unbound and bound toehold cover at equilibrium at 25 C. To do this we estimated the rate of toehold cover unbinding from its toehold domain:

$$k_{off} = k_{on} e^{\frac{\Delta G^\circ}{RT}} \quad (8)$$

The k_{off} value is 0.54 s^{-1}. At equilibrium, approximately 70% of the toehold is uncovered and the characteristic time for unbinding of the cleaved cover is $1/k_{off}$ or 1.86 seconds. Therefore, because the dynamics of hill pattern formation and recovery occured over a timescale of at least 10 hours and the timescale for equilibration of cleaved cover is under 10 seconds, we excluded toehold occlusion by the cleaved cover fragment in well-mixed models and reaction-diffusion models of hill pattern dynamics.

The final leak reaction we considered was reaction 8 (Figure S4). Initiator could bind to the exposed toehold on AHC and branch migrate to become partially hybridized to it. We assumed that Initiator reacted with AHC by hybridizing to its 7-nucleotide length toehold using the same literature value for the bimolecular rate constant assumed for 7 nt toehold mediated strand displacement reaction throughout this work, i.e. 3E6 M^{-1} s^{-1}. We incorporated this rate constant into hill pattern reaction-diffusion models as kh6. We also assumed that the Initiator:AHC complex could undergo branch migration and toehold unbinding to reform Initiator and AHC complex; we adapted the form of the effective unimolecular rate constant for this type of dissociation reaction which has been determined previously[4]:

$$k_{off} = k_{on} \frac{1}{N} e^{\frac{\Delta G^\circ}{RT}} \quad (9)$$

where N is the length of the branch migration domain available to Initiator for hybridization after toehold binding to form the three-strand intermediate complex. Here N has a length of 12 nucleotides. 1/N is a correction term that accounts for the number of iso-energetic branch migration states that contribute to the three-strand complex and accounts for the additional time the complex spends in these microstates, which lowers the rate of disassociation relative to that of a unimolecular reaction lacking these states. The dissociation rate constant of Initiator:AHC, kh7, as computed using Equation 9, is 0.045 s^{-1} at 25 ºC; this value was used in reaction-diffusion models.

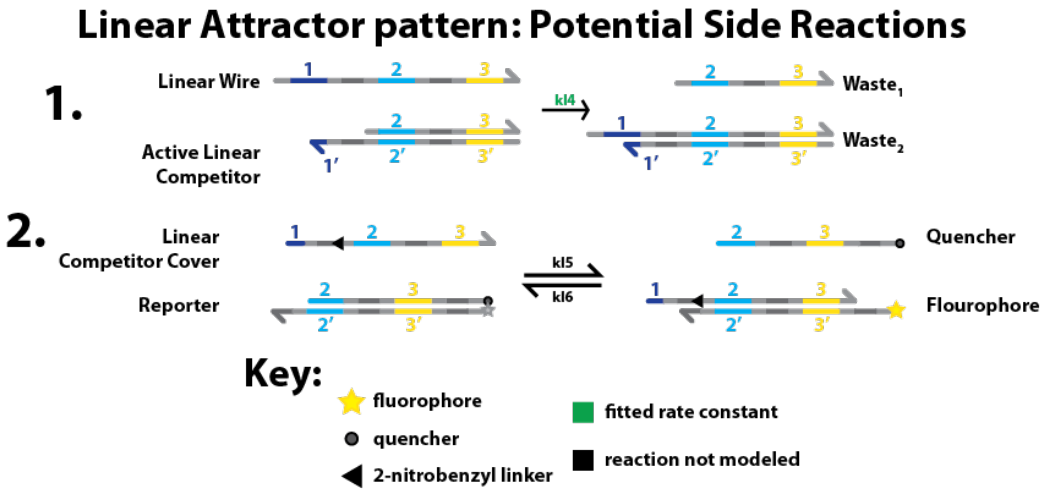

Figure S3. Unintended side reactions that could occur during linear pattern formation and recovery.

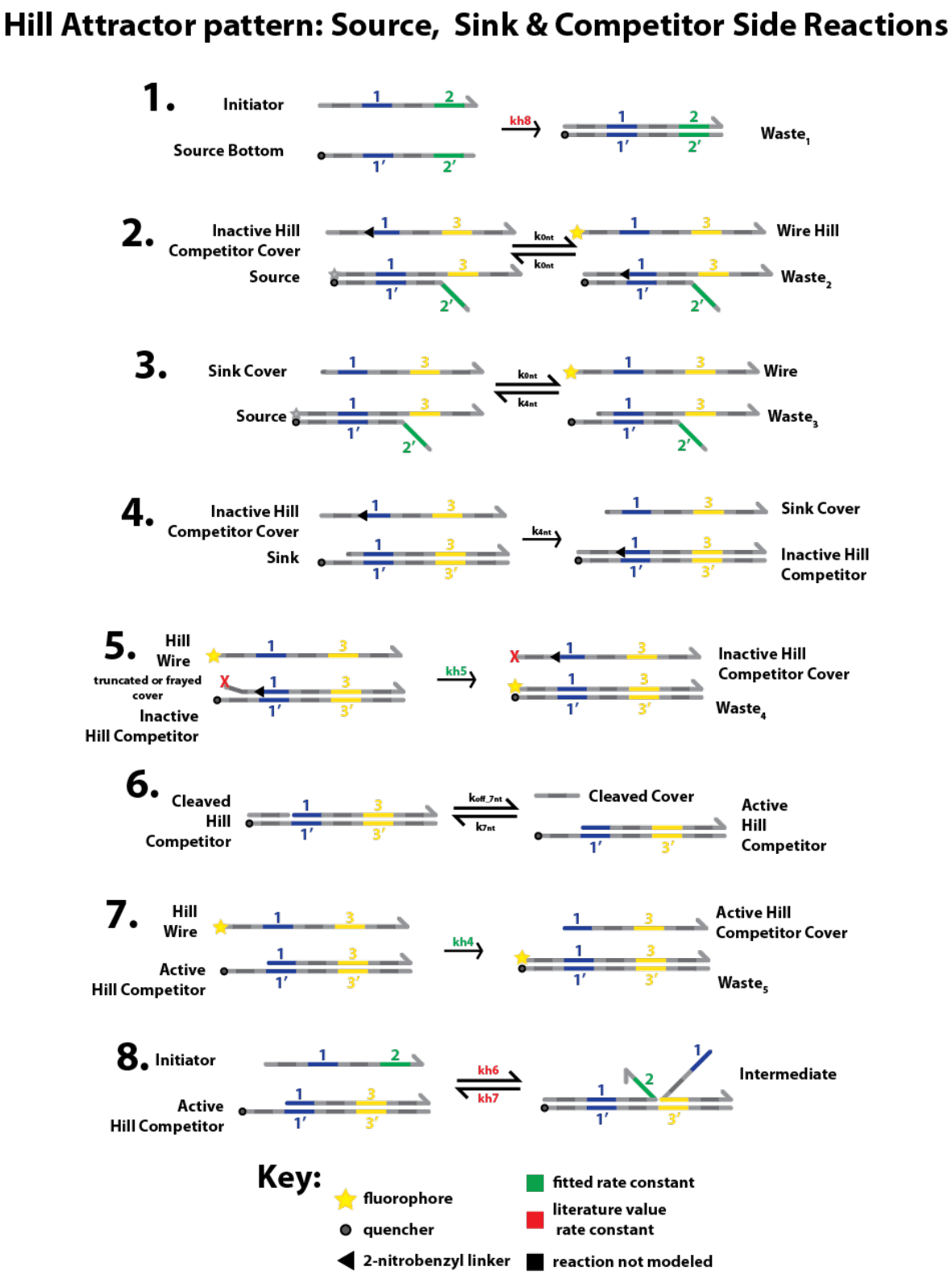

Figure S4. Unintended side reactions that could occur during hill pattern formation and recovery.

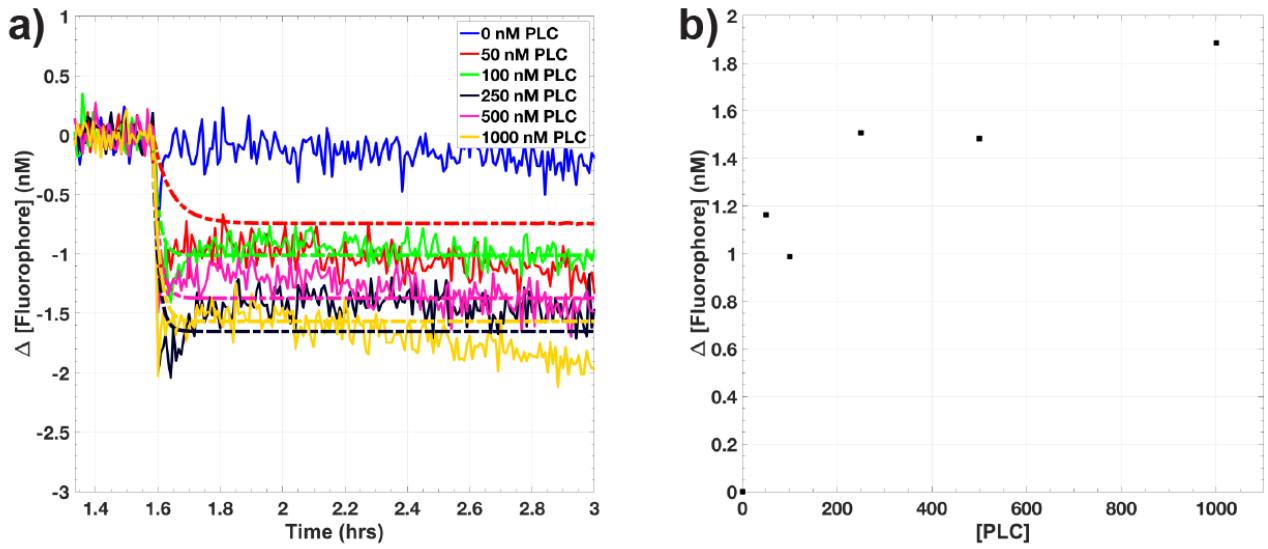

Figure S5. a) Addition of 0 to 1000 nM Pre-active Linear Competitor (PLC) to an equilibrated reaction of 200 nM Linear Wire (LW) and 20 nM Reporter. Dashed lines indicate results of the least squares fit of the ALC-LW leak rate constant kl4. b) Total change in Fluorophore concentration vs. concentration of PLC added to each reaction well.

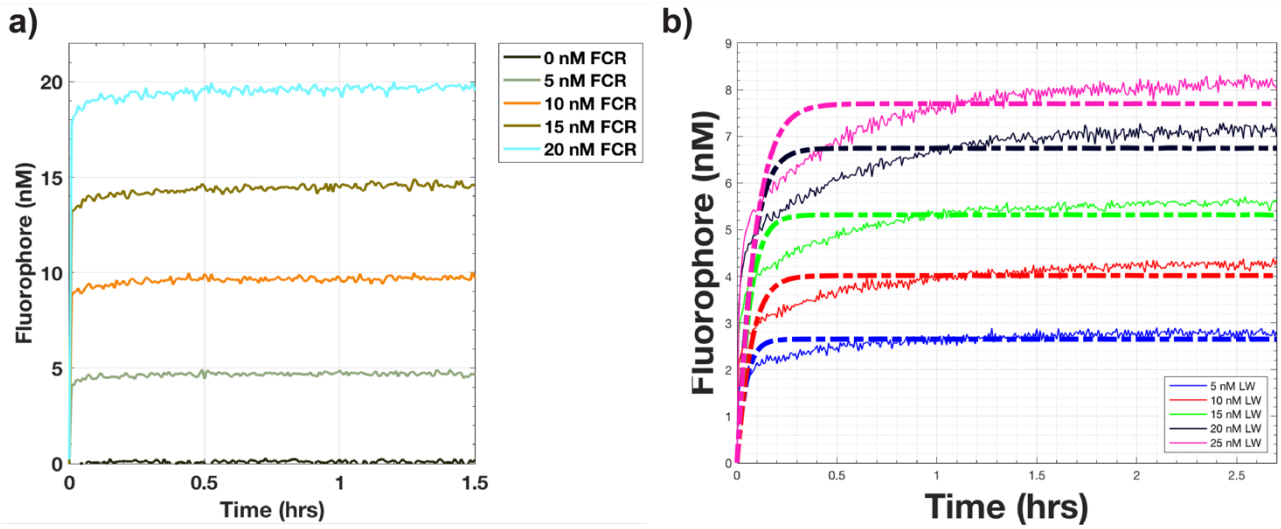

Figure S6. a) Addition of 0 to 20 nM Full Complement of the Reporter (FCR) to 20 nM of Reporter. b) Concentration of Fluorophore released after adding 5 to 25 nM of Wire to 20 nM Reporter. Dashed lines show results of least squares fit of model. These results were used to determine the concentration of Linear Wire (LW) released in characterizations of the leak reaction for the linear pattern network (See SI Section 4 text).

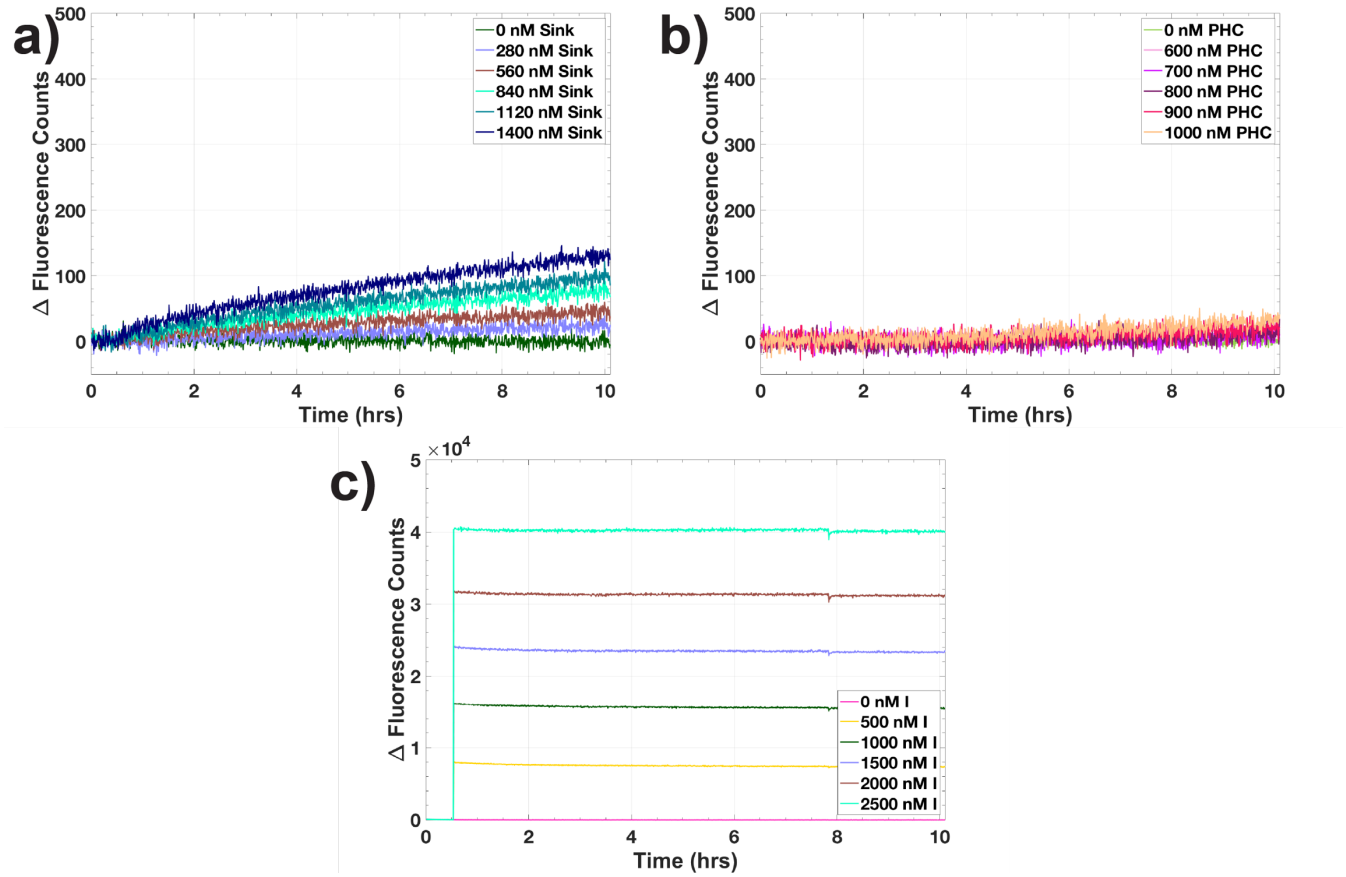

Figure S7. Changes in solution fluorescence intensity after a) 0 to 1400 nM Sink was added to 2500 nM Source, b) 0 to 1000 nM PHC was added to 2500 nM Source, c) 0 to 2500 nM Initiator (I) was added to 2500 nM Source.

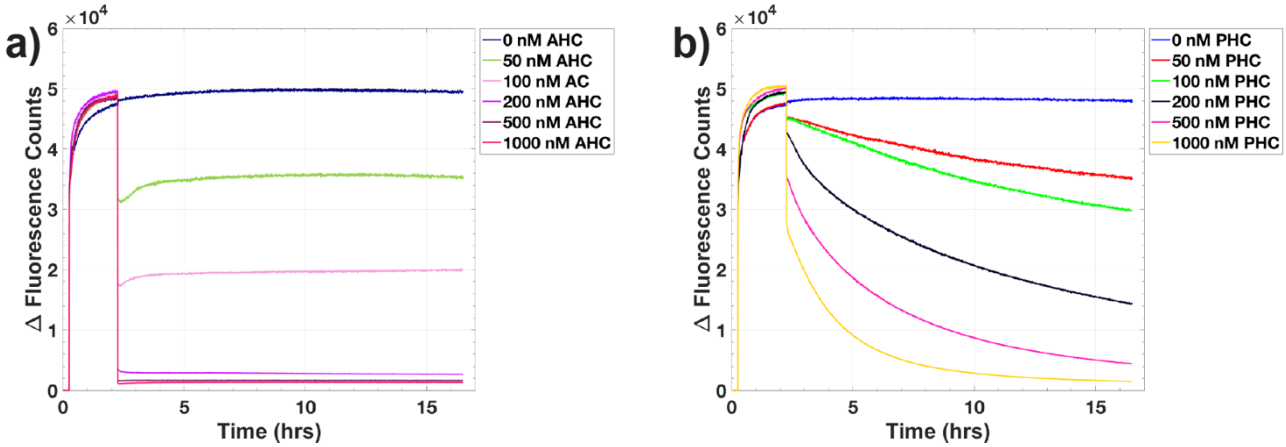

Figure S8. Changes in solution fluorescence intensity after a) 0 to 1000 nM Active Hill Competitor (AHC) was added to a solution containing 200 nM Source and 200 nM Initiator that were allowed to react to completion. b) 0 to 1000 nM Pre-active Hill Competitor (PHC) was added to a solution containing 200 nM Source and 200 nM Initiator that were allowed to react to completion.

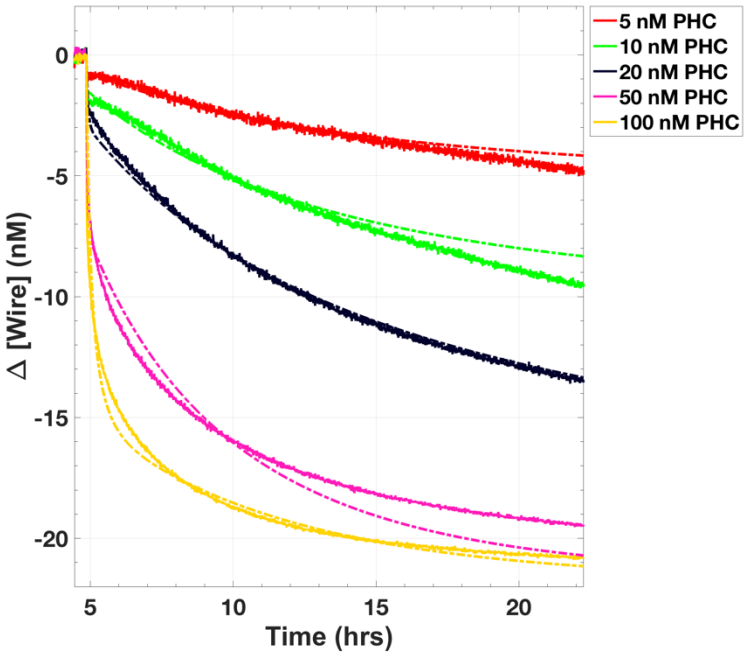

Figure S9. Measured changes in HW concentration after 5 to 100 nM PHC was added a solution where 22 nM Initiator and 20 nM Source were allowed to reaction to completion to produce 20 nM HW.

5. Reaction-Diffusion Models

Each model of a reaction-diffusion process consisted of a system of coupled 1-dimensional reaction-diffusion partial differential equations solved over a domain of 1500 microns. One reaction is included for each chemical species, where S_i, D_i and R_i are the species concentration, diffusion coefficient, and total reaction rate respectively:

$$\frac{\partial [S_i](t,x)}{\partial t} = D_i \nabla^2 [S_i](t,x) + R_i \quad (10)$$

The models were implemented in MATLAB.

Model Objectives:

For both linear and hill pattern systems, we first sought to use models of the reaction-diffusion processes to determine whether the proposed reactions coupled to diffusion of the species within a diffusion cell would produce stable patterns; we also sought to determine how fast patterns would form. Second, it was our objective to determine whether the experimental dynamics yielded rate constants and diffusion coefficients in reasonable agreement, within roughly an order of magnitude or so, of literature values for toehold-mediated strand displacement rate constants and measured values of DNA diffusion coefficients in 30%(v/v) PEDGA hydrogels to demonstrate that the observed dynamics were the result of the designed reaction networks. Lastly, using optimized parameters obtained by fitting the models to the experimental dynamics of pattern formation, we sought to establish whether the circuit recovered its original steady state in accordance with its intended behavior as an attractor pattern.

While designing the microfluidic platform, we initially used the 1-D models of hill pattern dynamics to decide on the dimensions required for the diffusion cells so that 1) the entire width of the hill patterns fit within the center third of the diffusion cell length and 2) to ensure that degradation of Wire occurred within the cell and to mitigate diffusive flux of Wire at the cell boundaries. Additionally, we selected the toeholds of the designed reactions and concentrations of supplied reactants to satisfy this condition. Both linear and hill pattern models initially used literature values for bimolecular and unimolecular strand displacement rate constants, and values of single and double stranded DNA diffusion coefficients measured in separate experiments (SI: Results & Discussion: Section 7 and Dorsey et al.[1]).

We then performed nonlinear least-squares regression to fit the rate constants of key reactions and fit ss and ds diffusion coefficients for all species to experimental formation data for both sets of patterns to. Again, it was our goal to determine whether the dynamics of the stable patterns we observed experimentally produced rate constants and diffusion coefficients in reasonable agreement, (to within roughly an order of magnitude) of known literature values for strand displacement reaction and DNA diffusivity. This agreement would support our claim that the observed dynamics of pattern formation were the result of the designed reaction networks. We then supplied the fitted parameters to the models as well as the pattern profile measured immediately after UV

perturbation as an initial condition from which the system could recover. Additionally, a parameter reflecting the fraction of UV-activated Competitor species within the UV-exposed section of a diffusion cell was also introduced as an initial condition to account for the presence of this species immediately following UV perturbation of patterns; a regression was performed to fit this parameter to the We compared the predicted timescale of recovery to the experimentally measured timescale of recovery with the objective that both recovery timescales should be on the same order of magnitude. Correspondence between recovery timescales would provide additional support for the designed systems' function as attractor patterns.

We used the built in MATLAB function *lsqnonlin* for all regression analyses of spatial patterns. We used this function to minimize the sum of the square of sum of the square of residuals over time between modeled fluorescence intensity profiles and experimental fluorescence intensity profiles over all points space and time. For example, if during pattern formation, y(x, t) represents a matrix holding all intensities measured at various points in space and time during this period, and $y_{fit}(x, t)$ represents a matrix holding predicted fluorescence intensities from the model based on a set of input parameters provided as a guess, the objective function minimized by *lsqnonlin* is:

$$Obj.Function = \sum_{x}\left(\sum_{t}\left(y(x,t) - y_{fit}(x,t)\right)^2\right)^2 \quad (11)$$

For a selected guess of input parameters, the residuals calculated at each x position and each time step were first squared to account for both positive and negative deviations of the model from the experimental data. The vectors of squared residuals were then summed over time to form an aggregate vector of squared residuals reflecting the total deviation of the model profiles from the experimental profiles at each x position over the full timescale being modeled. *lsqnonlin* took this vector as an argument and implicitly computed the sum of the squares of the vector and minimized this value according to the optimization constraints we provided.

During least-squares regression, the following general constraints were employed: the lower and upper bounds for fitted bimolecular rate constants were 0 M^{-1} s^{-1} and 4E6 M^{-1} s^{-1}; the lower and upper bounds for fitted ss and ds diffusion coefficients were 0 and 150 um^2 s^{-1}, which was chosen based on previous diffusion measurements of a 42 nucleotide strand in 30%(v/v) PEDGA hydrogels[1] where the magnitude of the diffusion coefficient was 60 ± 28 um^2 s^{-1} (mean ± standard deviation). All single stranded species were assigned the same single stranded diffusion coefficient. All double stranded species were assigned the same double stranded diffusion coefficient. β, a term that reflected the fraction of ILC or IHC converted to ALC or AHC immediately after UV perturbation within the exposed section of the diffusion cell, was allowed to vary between 0 and 1. Similarly, γ, an empirical term that reflected the relative contribution of Source complex to the total fluorescence intensity signal measured in hill pattern experiments, and accounted for imperfect quenching of the fluorophore within Source complex, was allowed to vary between 0 and 1. For each channel included in the fitting analysis (3 for linear patterns, and 5 for hill patterns), an initial guess was supplied; *lsqnonlin* was allowed to perform a total of 100,000 iterations in order to find a minimum. We observed that the choice of initial guess appeared to influence the convergence of the algorithm towards a particular solution. In order to verify that the set of optimized parameters presented in Tables S3 and S5 were suggestive of a global minimum and physically consistent with the toehold sizes, known mechanisms and rates of the DNA strand displacement reactions, we performed the fitting analyses multiple times where we gave *lsqnonlin* a different initial guess. Guesses were chosen to have rate constants that were inconsistent with the toehold sizes of in the CRN. We observed that the solution resulting from a guess that minimized the sum of the sum of the square of residuals, relative to other guesses, yielded rate constants that fell within one order of magnitude of theoretical values for rate constants predicted by Zhang and Winfree, which were based on toehold size. The sets of guesses and sets of parameters obtained from inconsistent guesses are listed in Table S5 and S6. Figures S10 and S11 show plots of the solution of linear and hill patterns obtained from these alternate guesses. Confidence intervals for the fitted parameters were obtained using the MATLAB function *nlparci*. All simulated results of linear and hill attractor pattern formation are presented in the main text figures and SI as dashed lines. We used the same definition of pattern formation and recovery timescale defined in the main text during discussion of model construction and dynamics in the sections below.

Linear Pattern Models:

The reaction-diffusion equations comprising the PDE model were:

$$\frac{\partial[LW](t,x)}{\partial t} = D_{ss}\nabla^2[LW](t,x) - k_{l1}[LW](t,x)[Reporter](t,x) - k_{l4}[LW](t,x)[ALC](t,x) + k_{l2}[Quencher](t,x)[Fluorophore](t,x)$$

$$\frac{\partial[Reporter](t,x)}{\partial t} = D_{ds}\nabla^2[Reporter](t,x) - k_{l1}[LW](t,x)[Reporter](t,x) + k_{l2}[Quencher](t,x)[Fluorophore](t,x)$$

$$\frac{\partial[Fluorophore](t,x)}{\partial t} = D_{ds}\nabla^2[Fluorophore](t,x) - k_{l2}[Quencher](t,x)[Fluorophore](t,x) + k_{l1}[LW](t,x)[Reporter](t,x)$$

$$\frac{\partial[Quencher](t,x)}{\partial t} = D_{ss}\nabla^2[Quencher](t,x) - k_{l2}[Quencher](t,x)[Fluorophore](t,x) + k_{l1}[LW](t,x)[Reporter](t,x)$$

$$\frac{\partial[ALC](t,x)}{\partial t} = D_{ds}\nabla^2[ALC](t,x) - k_{l4}[ALC](t,x)[LW](t,x)$$

The fit parameters for the linear pattern model were the forward and reverse Reporting rate constants (Figure 2a main text), kl1 and kl2, leak rate constant kl4 between Linear Wire (LW) and spuriously activated Competitor (ALC), and ss and ds diffusion coefficients for all species in the reaction network. The reaction rate constants kl1, kl2 and kl4 were estimated by fitting the nondimensionalized solution of the partial differential equation model to normalized experimental fluorescence profiles of pattern growth and stabilization (described below) using MATLAB's built-in *lsqnonlin* function. A single experimental fluorescence profile

consisted of a 1-dimensional vector of normalized fluorescence intensity pixels spanning the entire 1500 um length of a single diffusion cell at a given time point. The values of the profiles for a single pattern were normalized to the maximum and minimum intensities measured over all x-values and over all time points for that specific pattern so that the rescaled intensities ranged from 0 to 1. Fluorescence profiles for 7 individual time points were used to fit the model parameters to the normalized intensity data for a single pattern (main text Figure 3b). All single stranded species were assigned the same diffusion coefficient, D_{ss}. All double stranded species were assigned the same diffusion coefficient, D_{ds}. The initial concentrations of all species in the diffusion cells was 0. The concentrations of Pre-active Linear Competitor at the left and right boundaries of the diffusion cell were set to the concentrations used in the experiment. We set the right-side boundary concentrations of LW, Reporter, Quencher and Fluorophore species by assuming that the reporting reaction had reached equilibrium in the upstream reservoir; the initial reservoir concentrations of Reporter and LW (before the equilibration of the reporting reaction, Figure 3a, main text) were 400 nM and 500 nM; the equilibrated boundary concentrations of LW, Reporter, Quencher, and Fluorophore were determined from the definition of the reporting reaction equilibrium constant, K_{eq} = kl1/kl2, and incorporated mass balances reflecting the change in concentration, X, as a function of the initial concentration and fitted rate constants:

$$K_{eq} = \frac{[X][Quencher_0 + X]}{[Reporter_0 - X][LW_0 - X]} = \frac{kl1}{kl2} \quad (12)$$

Solving for the unknown X as a function for a particular set of rate constants and the known initial concentrations gives the concentrations of the different species at the right-hand boundary; the PDE model performed this calculation during regression.

The model incorporated the leak reaction between LW and spuriously generated ALC (Figure S3, Reaction 1) by assuming that this reaction went to completion within the upstream reservoir holding LW, Reporter, and PLC. We made this assumption about the reservoir concentrations because typically 1.5 hours passed between reservoir preparation and the start of an experiment, and well-mixed kinetic models predicted that the coupled reactions between LW and ALC and LW and Reporter reached steady state within 1 minute after initial mixing (Figure S10) assuming that the reactions proceeded with the fitted rate constants obtained from the experiments discussed in SI Results & Discussion: Section 4. Figure S10 shows how this assumption results in the same steady state as a system where the LW-ALC reaction is initiated at time t = 0. The reaction of 500 nM LW with 400 nM Reporter, 70 nM ALC (which is 7% of [PLC] = 1000 nM) and 40 nM Quencher are the dashed lines in the figure. After roughly 30 seconds, this reaction reaches the same concentrations as a reversible reporting reaction with initial concentrations of 430 nM LW, 400 nM Reporter, and 40 nM Quencher (solid lines), suggesting that the consumption of LW by 70 nM ALC, at long times, yields the same steady state solution as assuming an initial LW concentration of 430 nM, where 70 nM ALC has already reacted with an initial concentration of 500 nM Wire. As such, we assumed that no AC was present in the RHS reservoir and that its concentration at the RHS boundary of the diffusion cell was 0. At the LHS boundary, 7% of the PLC concentration was assumed to be ALC.

The average values of the fit-parameters are listed in Table S3. The predicted timescale of pattern formation was 3.2 hours, which was 24 minutes shorter than the experimentally observed timescale of formation of 3.6 hours. The fitted reporting rate constants for the reporting reaction, kl1 and kl2, were around 10^4 M^{-1} s^{-1}. The expected order of magnitude of a bimolecular rate constant for a 5-nt toehold is 10^4 M^{-1} s^{-1} [4]. We observed that the fitted value of kl4 strongly depended on the initial guess supplied during regression, when keeping the guesses for all other parameters constant. An initial guess of 1E4 M^{-1} s^{-1} resulted in an average fit value of 2.7E4 ± 1.6E4 M^{-1} s^{-1} (95% CI). An initial guess of 1.5E6 M^{-1} s^{-1}, based on the average value of kl4 determined in well-mixed experiments, resulted in an average fit value of 1.5E6 ± 1.5E4 M^{-1} s^{-1} (95% CI). Both values of rate constant kl4 did not appear to change the formation or recovery dynamics of the model; additionally, the fluorescence profiles predicted at each timepoint, as shown in Figure 3 and Figure 4 of the main text, appeared identical in both cases. The fitted value of kl4 determined in well-mixed experiments was 1.47E6 ± 0.052 M^{-1} s^{-1} (95% CI). This result suggested that the optimization phase space for kl4 was flat and that the system may be specified by kl1, kl2, and the single and double stranded diffusion coefficients.

Several additional factors could influence our estimation of kl4. First, the uncertainty in the fraction of ALC and ILC in the PLC mixture may have contributed to overestimation of the leak reaction rate in time at particular points in space. Additionally, the accuracy of the solution obtained from numerical integration and regression analysis could have been affected by noise in the fluorescence intensity profiles used to fit the model. Finally, by varying the choice of initial guess from the values listed in Table S3 to the example guesses provided in Table S4, we observed a relative increase of the magnitude of the minimized objective function by 1.4 and 209-fold respectively, suggesting that the parameters listed in Table S5 represent global minimization of the objective function. Figure S10 shows the plots of linear pattern formation with the results of the guesses listed in Table S4.

In Dorsey et al., the average diffusion coefficient for a 42 nucleotide long DNA strand was 60 ± 28 μm^2 sec^{-1} (± standard deviation)[1]. The mean of the fitted ss DNA diffusion coefficient was 59 ± 20 μm^2 sec^{-1} (95% CI) and fell within one standard deviation of mean value for single stranded DNA diffusion coefficients previously measured in 30% (v/v) PEGDA hydrogels[1]. The mean of the fitted ds DNA diffusion coefficient was 40 ± 10 μm^2 sec^{-1}(95% CI) and fell within one standard deviation of the mean value for a double stranded diffusion coefficient measured in a separate diffusion-only experiment in 30% (v/v) PEGDA hydrogels (see Results and Discussion 7 for measurement of ds DNA diffusion coefficient); the mean value of the ds diffusion coefficient was 26 ± 11 μm^{-1} s^{-1} (mean ± standard deviation).

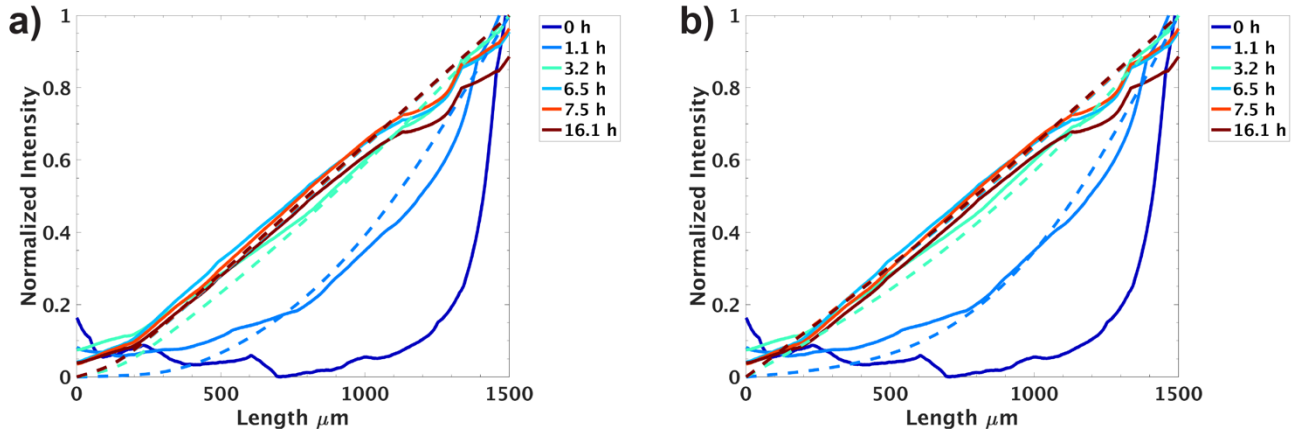

Figure S10. Plots of linear pattern formation for alternative parameter guesses: a) guess 2 and b) guess 3 listed in Table S4.

We then simulated linear pattern recovery after UV exposure using the rate constants and diffusion coefficients obtained from the dynamics of pattern formation. We performed nonlinear regression to fit a model of pattern recovery to the data. In addition to incorporating the constants obtained from the simulation of pattern formation, this model fit the fraction of ILC converted into ALC in the UV exposed region of the diffusion cell. This fraction, modelled by the parameter, β, had lower and upper bounds of 0 and 1 and was an applied to the model as a Heaviside step function multiplied by the steady state concentration of ILC. For example, if ILC(x) represented the steady state concentration profile of ILC within the diffusion cell prior to UV exposure, and UV exposure occurred between 125 μm ≤ x ≥ 625 μm, the transformed profile of ILC remaining at the conclusion of UV exposure, supplied as an initial concentration condition for the pattern recovery model after UV exposure, would be:

$$ILC_{postuv}(x, t = 0) = ILC(x)\big(1 - \beta\big(H(x - 125) + H(625 - x)\big) - \beta\big) \quad (13)$$

Similarly, the amount of ALC generated would be:

$$ALC_{generated} = ILC(x)\big(\beta\big(H(x - 125) + H(625 - x)\big) - \beta\big) \quad (14)$$

Figure S10 illustrates this transformation for an example profile.

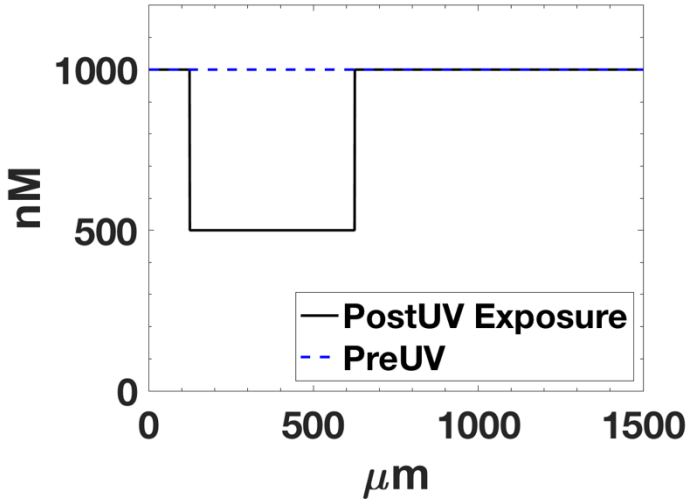

Figure S11. Transformation of an example concentration profile of 1000 nM with β = 0.5.

The model used the fluorescence intensity profile of the pattern present immediately after UV exposure as the initial Fluorophore concentration condition within the channel; this dimensionless intensity profile was converted into a Fluorophore concentration profile for the model by multiplying it by the Fluorophore concentration at the right boundary. β had a value of 1E-6 ± 6.8E-3 (95% CI) across all perturbations. Importantly, the model predicted pattern recovery in 2.2 hours after the first UV exposure which matched exactly with the 2.2 hrs experimental recovery timescale. For the 2nd and 3rd UV perturbations, the model predicted pattern stabilization within 1 hr and 2.1 hrs which were consistent with the experimentally observed timescales of 1.7 and 1.4 hours respectively. The model's ability to recapture experimental recovery timescales with a negligible value for β is indicative of the system's rapid equilibration following UV exposure as the loss of fluorescence is a direct indicator of the reaction of LW with ALC and the consumption of ALC within the diffusion cell. Although care was taken to resume fluorescence microscopy as quickly as possible after UV exposure with the DMD, reconfiguration of the microscope for imaging was performed manually and during this process,

upwards of 3-5 minutes may have passed between the termination of UV exposure and the resumption of imaging, resulting in a failure to capture the pattern degradation process. Overall, based on these results, we concluded that the proposed linear pattern reaction-diffusion mechanism recapitulated the experimentally observed formation and recovery dynamics.

Hill Pattern Models:

Reaction-diffusion models of hill pattern formation and recovery after UV-perturbation were set up following the same approach for modeling the formation and recovery of linear patterns. These models used the designed reactions and relevant leak reactions (see SI: Results & Discussion, Section 4) for the hill pattern formation process. The models were composed of the following partial differential equations:

$$\frac{\partial[HW](t,x)}{\partial t} = D_{ss}\nabla^2[Wire](t,x) - k_{h2}[HW](t,x)[Sink](t,x) - k_{h4}[HW](t,x)[AHC](t,x) - k_{h5}[HW](t,x)[IC](t,x) + k_{h1}[Source](t,x)[Initiator](t,x)$$

$$\frac{\partial[Source](t,x)}{\partial t} = D_{ds}\nabla^2[Source](t,x) - k_{h1}[Source](t,x)[Initiator](t,x)$$

$$\frac{\partial[Initiator](t,x)}{\partial t} = D_{ss}\nabla^2[Initiator]](t,x) - k_{h1}[Source](t,x)[Initiator](t,x) - k_{h5}[ACH](t,x)[Initiator](t,x) - k_{h8}[SB](t,x)[Initiator](t,x)$$

$$\frac{\partial[Sink](t,x)}{\partial t} = D_{ds}\nabla^2[Sink]](t,x) - k_{h2}[Sink](t,x)[HW](t,x)$$

$$\frac{\partial[IHC](t,x)}{\partial t} = D_{ds}\nabla^2[IHC]](t,x) - k_{h5}[IC](t,x)[HW](t,x)$$

$$\frac{\partial[AHC](t,x)}{\partial t} = D_{ds}\nabla^2[AHC]](t,x) - k_{h4}[AHC](t,x)[HW](t,x) - k_{h6}[AHC](t,x)[Initiator](t,x) + k_{h7}[Intermediate](t,x)$$

$$\frac{\partial[Intermediate](t,x)}{\partial t} = D_{ds}\nabla^2[Intermediate]](t,x) - k_{h7}[Intermediate](t,x) + k_{h6}[AHC](t,x)[Initiator](t,x)$$

$$\frac{\partial[SB](t,x)}{\partial t} = D_{ss}\nabla^2[SB](t,x) - k_{h8}[SB](t,x)[Initiator](t,x)$$

We first used this reaction-diffusion model to determine whether the observed dynamics of hill pattern formation (Figure 5b) were consistent with the designed reactions, and predicted rate constants and diffusion coefficients on the order of those expected from literature. The Hill Wire (HW) production rate constant, kh1, sink rate constant, kh2, and diffusion coefficients for ss and ds DNA D_{ss} and D_{ds} were fit to the measured fluorescence intensity profiles of hill pattern formation (Figure 5a, main text). All ss species were assigned the same ss DNA diffusion coefficient as a fit parameter; all ds complexes were assigned the same ds DNA diffusion coefficient as a fit parameter.

The leak rate constants for reactions between Wire and Inactive Hill Competitor (IHC), kh3, and Wire and Active Hill Competitor (AHC), kh4, measured in well-mixed solution were incorporated into the model as constants and assigned the value that was measured in well-mixed solution. Side reactions between excess Source Bottom strand (SB) and Initiator, and Initiator and AHC were assigned literature values for their bimolecular rate constants of kh8, and kh6 and kh7 based on the toehold size that initiated these reactions. kh8 was 3.5E6 M^{-1} s^{-1}, which is the biomolecular rate of two single oligos hybridizing at 25 ºC in standard buffer conditions[4]. For kh6 and kh7, spuriously active Competitor (AHC) binds and unbinds Initiator through toehold binding, branch migration, and unbinding. The value of kh6 and kh7 was 3E6 $M^{-1}s^{-1}$ and 0.045 s^{-1} as explained previously in discussion of reaction network characterization in well-mixed conditions. The concentration of AHC at each boundary was set to be 15% of the total Pre-active Hill Competitor (PHC) concentration with the remaining fraction being IHC (see SI Results & Discussion: Section 4). The initial concentrations of all species in the diffusion cell were set to 0. The concentrations of species on the boundary were set to be the same as those in experiments (Figure 5a). The model for the hill patterns also took into account the fact that the Source complex was imperfectly quenched, which created a linearly increasing fluorescence background signal, increasing from the left to the right-hand side of the hydrogel. To account for this effect in our model, we introduced an empirical parameter, γ, which was a scale factor between 0 and 1 reflecting the relative contribution of Source to the observed total fluorescence intensity. Therefore, the contribution of Source to the normalized intensity of fluorophore observed is:

$$Normalized\ Intensity(x,t) = \frac{[HW](x,t) + \gamma[Source](x,t)}{[HW](x_m,t_m) + \gamma[Source](x_m,t_m)} \quad (12)$$

where x_m, is the position where the summation of [HW] and γ*[Source] takes its maximum value which occurs at the peak position and t_m is the timepoint of the profile measured before the first UV perturbation.

The values of fitted parameters are listed in Table S6. The PDE model predicted pattern formation in roughly 4.3 hours which was within a factor of 2 of the average measured formation time of 6.7 ± 0.9 hrs. The expected values for kh1 and kh2 were 3E6 M^{-1} s^{-1} and 5E3 M^{-1} s^{-1}, which was based on the toeholds sizes for these reactions (7 nucleotides and 4 nucleotides respectively).[4] The mean values of fit parameters kh1 and kh2 obtained from the model were 2.4E6 ± 9E4 M^{-1} s^{-1} and 4.5E4 ± 60 M^{-1} s^{-1}, respectively

(Table S5). The average fitted value of kh1 matched the magnitude for the rate constant of a 7-nucleotide toehold initiated strand displacement reaction. The average fitted value of kh2 was also on the same order of magnitude as the expected rate constant for a 5-nt bimolecular toehold rate constant. Therefore, the fitted value of kh2 is a reasonable expectation for the specific design of the circuit. The fits to the ss and ds diffusion coefficients were 35 ± 0.4 um^2 s^{-1} and 23 ± 0.3 um^2 s^{-1} respectively (95% CI). The fit to the ss DNA diffusion coefficient was statistically consistent with a previously measured diffusion coefficient, 60 um^2 s^{-1} $\pm$ 28 um^2 s^{-1} (mean $\pm$ st. dev.), for ss DNA in 30%(v/v) PEGDA hydrogels[1]. The average value of the fitted ds DNA diffusion coefficient was also within 1 standard deviation of the diffusion coefficient for a ds complex that we measured (see SI Results & Discussion: Section 7). Additionally, by varying the choice of initial guess from the values listed in Table S5 to the example guesses provided in Table S6, we observed a relative increase of the magnitude of the minimized objective function by 354 and 638-fold respectively, suggesting that the parameters listed in Table S5 represent global minimization of the objective function.

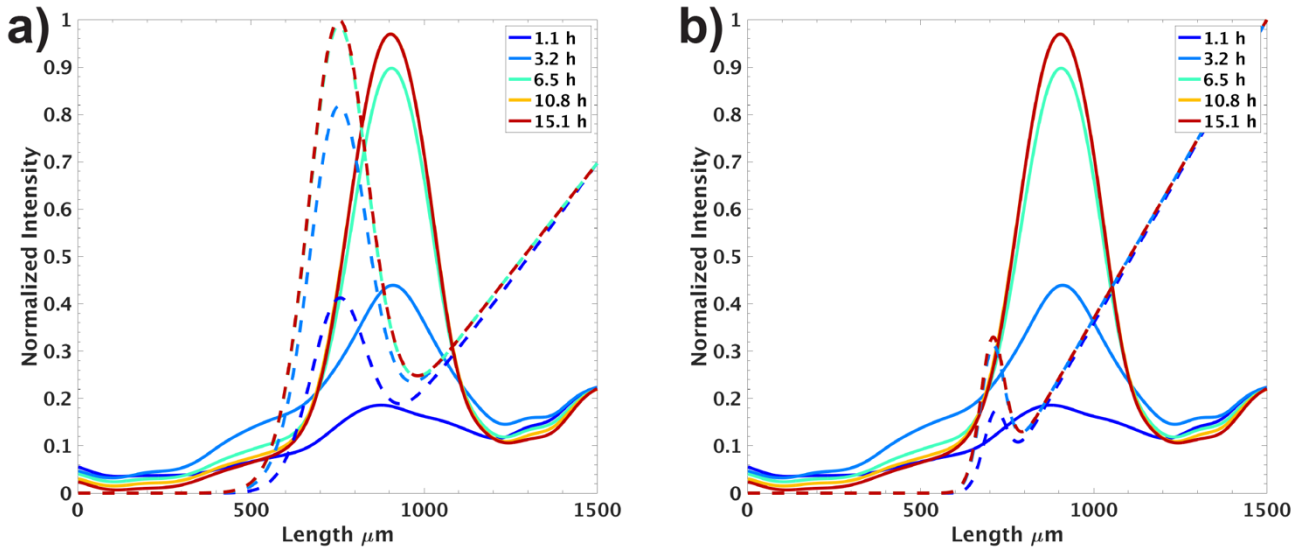

Figure S12. Plots of hill pattern formation for alternative parameter guesses: a) guess 2 and b) guess 3 listed in Table S6.

We simulated hill pattern recovery by supplying the model with the mean values of fit parameters kh1, kh2, D_{ss}, D_{ds}, and γ as constants; we performed nonlinear regression to fit the model of pattern recovery to the data using β as a fit parameter. The initial HW profile for the model was the fluorescence intensity profile measured immediately after UV perturbation (Figure 5c main text). The intensity profile was converted into Fluorophore concentration by re-arranging equation 12 to solve for the concentration of HW using γ, the steady state peak intensity, and the Source concentration profile at steady state, which was determined from the pattern formation model. The predicted dynamics are shown as normalized intensity in Figure 5c of the main text alongside the experimentally measure dynamics of pattern recovery. Recovery of the modeled pattern after perturbation took 2.1 hours to reach steady state; this recovery time differed by a factor of 2.5 from the recovery time of 5.2 hours measured in experiments. The value of β obtained from fitting was 0.99 ± 0.1, indicating that 99% of the IHC present within the portion of the diffusion cell exposed to UV was converted to AHC. The predicted timescale of recovery was within an order of magnitude of the experimental timescale, which again captures the level of accuracy we sought to attain through our models as the rate constants were approximated, using reaction diffusion processes (which do not take explicitly into account DNA toehold hybridization sequence composition and binding strength) to roughly an order of magnitude based on spatiotemporal dynamics and estimated reaction rates [4].

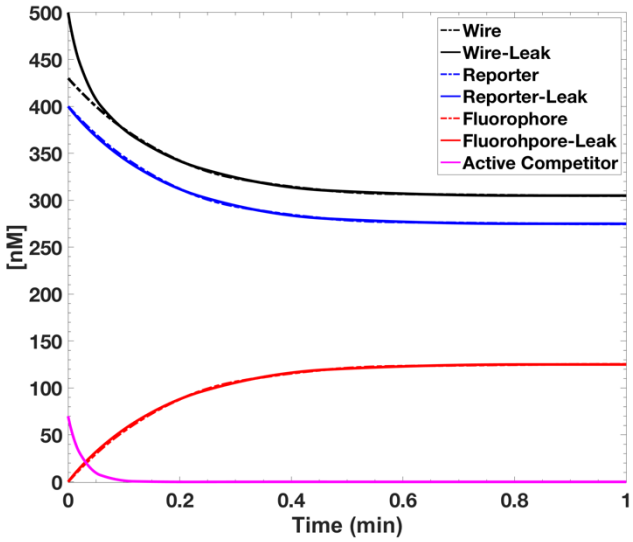

Figure S13. A well-mixed reservoir reaction model of LW-ALC leak. Dashed lines: initial concentrations of 500 nM LW, 400 nM Reporter, 40 nM Quencher, and 70 nM ALC. Solid lines: 200 nM LW, 400 nM Reporter, 40 nM Quencher.

Table S3. Average Linear pattern fit parameters (95%CI)

Parameters	kl1	kl2	kl4	D_{ss}	D_{ds}	β
Fitted value	5.6E4 ± 0.9 E4 M^{-1} s^{-1}	4.5E5 ± 1.0E5 M^{-1} s^{-1}	2.7E4 ± 1.6E4 M^{-1} s^{-1}	59 ± 20 μm^2 s^{-1}	40 ± 10 μm^2 s^{-1}	1E-6 ± 6.8E-3
Guess	6E4 M^{-1} s^{-1}	5E4 M^{-1} s^{-1}	1E4 M^{-1} s^{-1}	60 μm^2 s^{-1}	40 μm^2 s^{-1}	0.5

Table S4. Alternate guesses and average Linear pattern fit parameters (95%CI). The objective function column shows the X-fold increase occurring in the objective function resulting from the example guesses provided.

Parameters	kl1	kl2	kl4	D_{ss}	D_{ds}	Obj. Fnct.
Ex. Guess 2	1E2 M^{-1} s^{-1}	3E2 M^{-1} s^{-1}	3E3 M^{-1} s^{-1}	50 μm^2 s^{-1}	50 μm^2 s^{-1}	N/A
Fitted value	81 ± 160 M^{-1} s^{-1}	16 ± 20 M^{-1} s^{-1}	4E6 ± 1E7 M^{-1} s^{-1}	61 ± 83 μm^2 s^{-1}	40 ± 14 μm^2 s^{-1}	1.4X
Ex. Guess 3	3E4 M^{-1} s^{-1}	10 M^{-1} s^{-1}	4E6 M^{-1} s^{-1}	90 μm^2 s^{-1}	60 μm^2 s^{-1}	N/A
Fitted value	4E5 ± 1E4 M^{-1} s^{-1}	3.5E6 ± 5E3 M^{-1} s^{-1}	10 ± 0.2 M^{-1} s^{-1}	49 ± 0.1 μm^2 s^{-1}	50 ± 0.1μm^2 s^{-1}	209X

Table S5. Average Hill pattern fit parameters (95%CI)

Parameters	kh1	kh2	D_{ss}	D_{ds}	γ	β
Fitted value	2.4E6 ± 9E4 M^{-1} s^{-1}	3.2E3 ± 60 M^{-1} s^{-1}	35 ± 0.4 μm^2 s^{-1}	23 ± 0.30 μm^2 s^{-1}	1.3E-2 ± 2E-3	0.99 ± 0.1
Guess	2E6 M^{-1} s^{-1}	3E3 M^{-1} s^{-1}	35 μm^2 s^{-1}	23 μm^2 s^{-1}	1.3E-2	0.5

Table S6. Alternate guesses and average Hill pattern fit parameters (95%CI). The objective function column shows the X-fold increase occurring in the objective function resulting from the example guesses provided.

Parameters	kh1	kh2	D_{ss}	D_{ds}	γ	Obj. Fnct.
Ex. Guess 2	1E5 M^{-1} s^{-1}	4E4 M^{-1} s^{-1}	50 μm^2 s^{-1}	50 μm^2 s^{-1}	1.25E-2	N/A
Fitted value	1.0E5 ± 1.0E3 M^{-1} s^{-1}	4.0E4 ± 1E3 M^{-1} s^{-1}	50 ± 0.35 μm^2 s^{-1}	50 ± 0.1 μm^2 s^{-1}	1.25E-2 ± 7E-4	354X
Ex. Guess 3	1E2 M^{-1} s^{-1}	1E6 M^{-1} s^{-1}	80 μm^2 s^{-1}	90 μm^2 s^{-1}	1.25E-2	N/A
Fitted value	2.0E6 ± 5.0E6 M^{-1} s^{-1}	1.0E6 ± 1.0E6 M^{-1} s^{-1}	80 ± 12 μm^2 s^{-1}	90 ± 19 μm^2 s^{-1}	1.25E-2± 1.25E-2	638X

6. Times for the average Peak Intensity of hill-shaped patterns to return to within 10% of steady state peak intensity after repeated UV-induced perturbation

The range of the recovery times was 3.3 hours respectively for the first and second perturbations. The average time across all 4 patterns to return to 10% of the final measured steady state before any UV perturbation was 7.1 hrs for the first perturbation and 7.0 hrs for the second perturbation.

Table S7. Measured times for normalized peak intensities to return to within 10% of its maximum value after pattern perturbation

	Cell 1	**Cell 2**	**Cell 3**	**Cell 4**
First perturbation	9.8 hrs	6.5 hrs	5.4 hrs	6.5 hrs
Second perturbation	9.7 hrs	6.5 hrs	5.4 hrs	6.5 hrs

7. Measuring the diffusion coefficient for double stranded DNA in the hydrogel medium

We measured the diffusion coefficient of 31 base-pair ds DNA in 30%(v/v) PEGDA hydrogels. Wire:Sink(noQ) was allowed to diffuse into hydrogels patterned within diffusion cells by setting the boundary concentrations to 200 nM Wire:Sink(noQ) at the right sides of the cells and 0 nM at the left sides of the cells. The diffusion coefficient for Wire:Sink(noQ) within the hydrogels was determined using *lsqnonlin* and the process described in section 5; we fit the diffusion coefficient using nonlinear least-squares regression to the solution of the 1-D diffusion equation with homogeneous boundary conditions. A graph of the diffusion profile and fit are shown in Figure S11. The fitted diffusion coefficient was 26 ± 11 μm^{-1} s^{-1} (mean ± standard deviation).

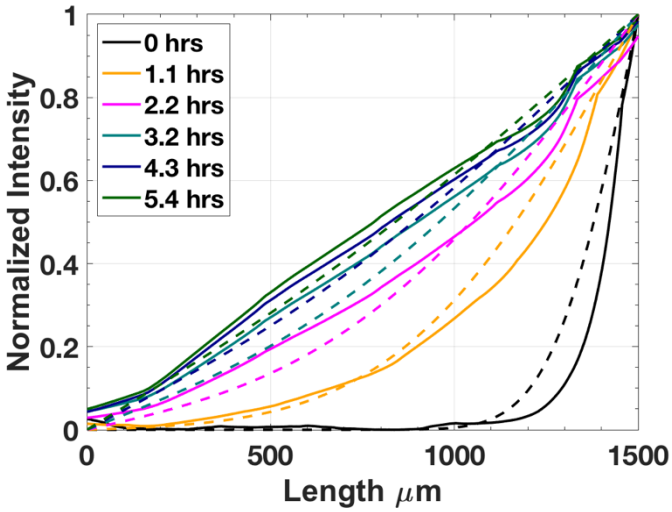

Figure S14. Formation of a diffusive gradient of the Hill Wire:Source(noQ) complex in a diffusion cell. The boundary conditions consisted of a solution of 200 nM of the Hill Wire:Sink(noQ) complex in 1X TAE /Mg^{2+} buffer at the right side boundary and buffer with no DNA at the left side boundary. Solid lines indicate experimental data while dashed lines indicate the least-squares fit to the solution of the 1-D diffusion equation with homogenous boundary conditions[1].

References

[1] P. J. Dorsey, M. Rubanov, W. Wang, R. Schulman, *ACS Macro Lett.* **2019**, *8*, 1133–1140.

[2] N. Mavrogiannis, M. Ibo, X. Fu, F. Crivellari, Z. Gagnon, *Biomicrofluidics* **2016**, *10*, 34107.

[3] D. Y. Zhang, A. J. Turberfield, B. Yurke, E. Winfree, *Science.* **2007**, *318*, 1121–1125.

[4] D. Y. Zhang, E. Winfree, *J. Am. Chem. Soc.* **2009**, *131*, 17303–17314.

[5] Y. You, A. V Tataurov, R. Owczarzy, *Biopolymers* **2011**, *95*, 472–486.

[6] B. G. Moreira, Y. You, M. A. Behlke, R. Owczarzy, *Biochem. Biophys. Res. Commun.* **2005**, *327*, 473–484.

Author Contributions

PJD and RS designed the experiments. PJD conducted the experiments and simulations. DS provided conceptual & technical advice. PJD performed the data analyses and PJD and RS wrote the paper.